## Superfluid, solid, supersolid and quantum phase transitions on bipartite lattices and its applications on ultra-cold atoms on optical lattices, adatom adsorption on substrates and high temperature superconductors

#### Jinwu Ye

Department of Physics, The Pennsylvania State University, University Park, PA, 16802 (Dated: November 7, 2018)

We study phases such as superfluid, solid, supersolid and quantum phase transitions in a unified scheme in extended boson Hubbard models slightly away from half filling on bipartite optical lattices such as honeycomb and square lattice. We also map out its global phase diagram at T=0. We find that in the translational symmetry breaking side, different kinds of supersolids are generic possible states slightly away from half filling. We propose a new kind of supersolid: valence bond supersolid. We show that the quantum phase transitions from solids to supersolids driven by a chemical potential are in the same universality class as that from a Mott insulator to a superfluid, therefore have exact exponents  $z=2, \nu=1/2, n=0$  with a logarithmic correction. Comparisons with previous quantum Monte-Carlo (QMC) simulations on a square lattice are made. Implications on possible future QMC simulations are given. All these phases and phase transitions can be realized in ultra-cold atoms loaded on optical bipartite lattices. Then we use our results to study the reentrant "superfluid" in a narrow region of coverages in the second layer of  ${}^4He$  adsorbed on graphite and the low temperature phase diagram of Hydrogen physisorbed on Krypton-preplated graphite ( $H_2/Kr/graphite$ ) near half filling. We suggest that  ${}^4He$  and  $H_2$  lattice supersolids maybe responsible for the experimental signals in the two systems. Finally, we suggest Cooper supersolid is repressible for the phase diagram of  $La_{2-x}Ba_xCuO_4$  near x=1/8.

KITP report No. NSF-KITP-05-14

### I. INTRODUCTION.

The Boson Hubbard model with various kinds of interactions, on all kinds of lattices and at different filling factors is described by the following Hamiltonian<sup>1</sup>:

$$H = -t \sum_{\langle ij \rangle} (b_i^{\dagger} b_j + h.c.) - \mu \sum_i n_i + \frac{U}{2} \sum_i n_i (n_i - 1)$$

$$+ V_1 \sum_{\langle ij \rangle} n_i n_j + V_2 \sum_{\langle \langle ik \rangle \rangle} n_i n_k + \cdots$$
(1)

where  $n_i = b_i^{\dagger} b_i$  is the boson density, t is the nearest neighbor hopping which is determined by the depth of the trapping potential at the preferred adsorption sites.  $U, V_1, V_2$  are onsite, nearest neighbor (nn) and next nearest neighbor (nnn) interactions respectively, the  $\cdots$  may include further neighbor interactions and possible ring-exchange interactions.

In the hard-core limit  $U \to \infty$ , due to the exact mapping between the boson operator and the spin s=1/2 operator:  $b_i^{\dagger} = S_i^+, b_i = S_i^-, n_i = S_i^z + 1/2$ , the boson model Eqn.1 can be mapped to a "generalized" anisotropic S=1/2 quantum Heisenberg model in an external magnetic field<sup>16,48</sup>:

$$H = -2t \sum_{\langle ij \rangle} (S_i^x S_j^x + S_i^y S_j^y)$$

$$+ V_1 \sum_{\langle ij \rangle} S_i^z S_j^z + V_2 \sum_{\langle \langle ik \rangle \rangle} S_i^z S_k^z - h \sum_i S_i^z + \cdot (2)$$

where  $h = \mu - 2V_1 - 2V_2$  for a square lattice and the  $\cdots$  may include further neighbor interactions and ring-exchange interactions.

The model Eqn.1 with only the onsite interaction was first studied in Ref.<sup>1</sup>. It was found that there is a second order superconductor to insulator transition at filling factor f = 1, while away from f = 1, the system can only be in the superfluid state. The effects of long range Coulomb interactions on the transition was studied in  $^{2,3}$ . Recently, a dual vortex method (DVM) in<sup>4</sup> was developed to study Eqn.1 on a square lattice at generic commensurate filling factors f=p/q ( p,q are relative prime numbers ). After performing the charge-vortex duality transformation<sup>7</sup>, the authors in<sup>4</sup> obtained a dual theory of Eqn.1 in term of the interacting vortices  $\psi_a$  hopping on the dual lattice subject to a fluctuating dual" magnetic field". The average strength of the dual " magnetic field " through a dual plaquette is equal to the boson density f = p/q. This is similar to the Hofstadter problem of electrons moving in a crystal lattice in the presence of a magnetic field<sup>8,9</sup>. The projective representation of the space group (PSG) dictates that there are at least q-fold degenerate minima in the mean field energy spectrum. Near the superconductor to the insulator transition, the most important  $\psi_a$  fluctuations will be near these q minima which can be labeled as  $\psi_l, l = 0, 1, \dots, q-1$  which forms a q dimensional representation of the PSG. In the continuum limit, the final effective theory in terms of these q order parameters should be invariant under this PSG. In the superfluid state  $\langle \psi_l \rangle = 0$  for every l, while in the insulating state  $\langle \psi_l \rangle \neq 0$  for at least one l. In the insulating state, there must exist some kinds of charge density wave (CDW) or valence bond solid ( VBS) states which may be stabilized by longer range interactions or possible ring exchange interactions included in Eqn.1. The CDW or VBS order parameter was constructed to be the most general *bilinear* and gauge invariant combinations of the  $\psi_l^4$ .

In a recent unpublished preprint<sup>20</sup>, the author studied all the possible phases and phase transitions in the EBHM slightly away from half filling q=2 on bipartite lattices such as honeycomb and square lattice. It was established in  $^{20}$  that the dual vortex method at d=2 can achieve many important results which are very hard to get from the direct boson picture. Although square lattice has been studied by various analytic and numerical methods before, the boson Hubbard model on a honeycomb lattice was not studied in any details by both analytic and Quantum Monte-Carlo (QMC) methods before the preprint<sup>20</sup>. It is not a Bravais lattice, so may show some different properties than those in square lattice. Experimentally, the honeycomb lattice maybe the relevant lattice for adatom adsorption on substrates. The honevcomb lattice could also be easily realized in ultra-cold atomic experiments. It was found that a supersolid ( SS) state exists only away from half filling. A supersolid in Eqn. 1 is a state with both superfluid and solid order. A supersolid in Eqn.2 is defined as the simultaneous orderings of ferromagnet in the XY component ( namely,  $\langle b_i \rangle \neq 0$ ) and CDW in the Z component. Recently, by using the torsional oscillator measurement, a PSU's group lead by Chan observed a marked  $1 \sim 2\%$  superfluid component even in bulk solid  ${}^4He$  at  $\sim 0.2K^{10}$ . If this experimental observation indicates the existence of <sup>4</sup>He supersolid remains controversial<sup>11</sup>. However, it was established by spin wave  $expansion^{12}$  and quantumMonte-carlo (QMC)<sup>13,14,15</sup> simulations that a supersolid state could exist in an extended boson Hubbard model (EBHM) with suitable lattice structures, filling factors, interaction ranges and strengths. It was also explicitly pointed out in<sup>20</sup> that the DVM developed in<sup>4</sup> holds only in the superfluid (SF) and the valence bond solid (VBS ) side where the saddle point of the dual gauge field can be taken as uniform, however, it fails in the charge density wave (CDW) side where the saddle point of the dual gauge field can not be taken as uniform anymore. Special care is needed to choose a correct saddle point of the dual gauge field in the CDW side, so a different action is needed in the CDW side<sup>20</sup>. This paper is an expanded version of the unpublished preprint<sup>20</sup>. In this expanded version, (1) by pushing the DVM to slightly away from commensurate filling factors and (2) also extending the DVM explicitly to the lattice symmetry breaking side by choosing the corresponding saddle points of the dual gauge field, I will map out the global phase diagram of the EBHM on bipartite optical lattices such as honeycome and square lattice near half filling and also investigate superfluid, solid, especially supersolids and quantum phase transitions in the phase diagram in a unified scheme. The DVM is a magnetic space group ( MSG )<sup>4</sup> symmetry-based approach which, in principle, can be used to classify all the possible phases and phase transitions. But the question if a particular phase will appear or not as a ground state depends on the specific values of all the possible parameters in the EBHM in Eqn.1, so it can only be addressed by a microscopic approach such as Quantum Monte-Carlo (QMC) simulations. The DVM can guide the QMC to search for particular phases and phase transitions in a specific model. Finite size scalings in QMC in a microscopic model can be used to confirm the phases and the universality classes of phase transitions discovered by the DVM. The two methods are complementary to each other and both are needed to completely understand phases and phase transitions in Eqn.1. In this paper, we will also compare our results achieved by the DVM with some available QMC results and make implications on possible future QMC simulations. Then we study the application of our results on 3 different experimental systems: ultra-cold atoms with long range interactions on optical lattices in both square and honeycomb lattice, adatom adsorption on different substrates such as possible reentrant supersolids in the second layer of <sup>4</sup>He adsorbed on graphite and Hydrogen adsorbed on Krypton-preplated graphite in honeycomb lattice, possible cooper pair supersolid in high temperature superconductor  $La_{2-x}Ba_xCuO_4$  in square lattice.

## II. MAGNETIC SPACE GROUP, EFFECTIVE ACTION AND ORDER PARAMETERS IN THE DUAL VORTEX PICTURE.

In this section, we will extend the DVM in<sup>4</sup> to study the EBHM Eqn.1 in honeycomb lattice at and slightly away from q = 2. Honeycomb lattice (solid line in Fig.1) is not a Bravais lattice, so may show some different properties than a square lattice. The dual lattice of the honeycomb lattice is a triangular lattice ( dashed line in Fig.1). Two basis vectors of a primitive unit cell of the triangular lattice can be chosen as  $\vec{a}_1=\hat{x}, \vec{a}_2=-\frac{1}{2}\hat{x}+\frac{\sqrt{3}}{2}\hat{y}, \vec{a}_d=\vec{a}_1+\vec{a}_2$  as shown in Fig.1. The reciprocal lattice of a triangular is also a triangular lattice and spanned by two basis vectors  $\vec{k} = k_1 \vec{b}_1 + k_2 \vec{b}_2$  with  $\vec{b}_1 = \hat{x} + \frac{\hat{y}}{\sqrt{3}}, \vec{b}_2 = \frac{2}{\sqrt{3}} \hat{y}$  satisfying  $\vec{b}_i \cdot \vec{a}_j = \delta_{ij}$ . The point group of a triangular lattice is  $C_{6v} \sim D_6$  which contains 12 elements. The two generators can be chosen as  $C_6 = R_{\pi/3}, I_1$ . The space group also includes the two translation operators along  $\vec{a}_1$  and  $\vec{a}_2$  directions  $T_1$  and  $T_2$ . The 3 translation operators  $T_1, T_2, T_d$ , the rotation operator  $R_{\pi/3}$ , the 3 reflection operators  $I_1, I_2, I_d$ , the two rotation operators around the direct lattice points Aand B:  $R_{2\pi/3}^A$ ,  $R_{2\pi/3}^B$  of the MSG are worked out in the following.

In the Landau gauge  $\vec{A} = (0, Hx)$ , the mean field Hamiltonian for the vortices hopping in a triangular lattice in the presence of f flux quanta per triangle in the

tight-binding limit is $^4$ :

$$H_{0v} = -t \sum_{\vec{x}} [|\vec{x} + \vec{a}_1| > < \vec{x}| + h.c.$$

$$+ |\vec{x} + \vec{a}_2| > e^{i2\pi 2fa_1} < \vec{x}| + h.c.$$

$$+ |\vec{x} + \vec{a}_d| > e^{i2\pi 2f(a_1 + 1/2)} < \vec{x}| + h.c.]$$
(3)

where  $\vec{x} = a_1 \vec{a}_1 + a_2 \vec{a}_2$  denotes lattice points of the triangular lattice. Note that the total vortex Hamiltonian  $H_v = H_{0v} + V$  where V is the interaction between vortices. Because V does not contain any Aharonov-Bohm (AB) phase factor from the non-trivial  $A_{\mu}$  background, so the magnetic space group is completely determined by the vortex kinetic term  $H_{0v}$ . V always commutes with the generators of the MSG given by Eqns. 4,5,10. So when constructing the representation of the MSG, we can ignore the V term without losing any generality.

The  $T_1, T_2, T_d$  and the rotation operator  $R_{\pi/3}$  of the PSG are worked out in<sup>4</sup>. Here we listed them in slightly different notations:

$$T_{1} = \sum_{\vec{x}} |\vec{x} + \vec{a}_{1} > e^{i2\pi^{2}fa_{2}} < \vec{x}|$$

$$T_{2} = \sum_{\vec{x}} |\vec{x} + \vec{a}_{2} > < \vec{x}|$$

$$T_{d} = \sum_{\vec{x}} |\vec{x} + \vec{a}_{d} > e^{i2\pi^{2}f(a_{2} + 1/2)} < \vec{x}|$$

$$R_{\pi/3} = \sum_{\vec{x}} e^{i2\pi f(a_{1}^{2} - 2a_{1}a_{2})} |a_{1} - a_{2}, a_{1} > < a_{1}, a_{2}|$$
(4)

It can be shown that they all commute with H. However, they do not commute with each other  $T_1T_2 = \omega T_d, T_1T_2 = \omega^2 T_2 T_1$ .

After performing some algebras, we found three of the 6 reflection operators in the point group  $C_{6v}$ :

$$I_{1} = K \sum_{\vec{x}} e^{-i2\pi f a_{2}^{2}} |a_{1} - a_{2}, -a_{2}\rangle \langle a_{1}, a_{2}|$$

$$I_{2} = K \sum_{\vec{x}} e^{-i2\pi f a_{1}^{2}} |-a_{1}, a_{2} - a_{1}\rangle \langle a_{1}, a_{2}|$$

$$I_{d} = K \sum_{\vec{x}} e^{-i2\pi f 2a_{1}a_{2}} |a_{2}, a_{1}\rangle \langle a_{1}, a_{2}|$$
(5)

where K is the complex conjugate operator which make  $I_1, I_2, I_3$  non-unitary operators. Note that in contrast to the reflection operators in square lattice, the phase factors in Eqn.5 are crucial to ensure they commute with the Hamiltonian Eqn.3.

The eigenvalue equation  $H\psi(\vec{k}) = E(\vec{k})\psi(\vec{k})$  leads to the Harper's equation in the triangle lattice:

$$(e^{-ik_1} + e^{-i(k_1+k_2+2\pi f(2l-1))})\psi_{l-1}(k_1, k_2)$$

$$+(e^{ik_1} + e^{i(k_1+k_2+2\pi f(2l-1))})\psi_{l+1}(k_1, k_2)$$

$$+2\cos(-k_2 + 2\pi f l)\psi_l(k_1, k_2) = E(\vec{k})\psi_l(k_1, k_2)$$
 (6)

where  $l = 0, 1, \dots, q - 1$ .

In the following, we focus on q=2 case where there is only one band  $E(\vec{k})=-2t(\cos k_1+\cos k_2-\cos(k_1+k_2))$ . Obviously,  $E(k_1,k_2)=E(-k_1,-k_2)=E(k_2,k_1)$ . There are two minima at  $\vec{k}_{\pm}=\pm(\pi/3,\pi/3)$ . Let's label the two eigenmodes at the two minima as  $\psi_{\pm}$ . By using the expressions of the rotation and reflection operators in Eqns. 4, 5, we find the two fields transform as:

$$T_1, T_2 : \psi_{\pm} \to e^{\mp i\pi/3} \psi_{\pm}; \quad T_d : \psi_{\pm} \to -e^{\mp i2\pi/3} \psi_{\pm}$$
  
 $R_{\pi/3} : \psi_{\pm} \to \psi_{\mp}; \quad I_{\alpha} \psi_{\pm} \to \psi_{\pm}^*, \quad \alpha = 1, 2, d \quad (7)$ 

where the transformations under  $T_{\alpha}$ ,  $R_{\pi/3}$  were already derived in<sup>4</sup>.

The quadratic terms of the effective action is simply the scalar electrodynamics as in the square lattice case:

$$\mathcal{L}_0 = \sum_{\alpha = +} |(\partial_{\mu} - iA_{\mu})\psi_{\alpha}|^2 + r|\psi_{\alpha}|^2 + \frac{1}{4}F_{\mu\nu}^2$$
 (8)

where  $F_{\mu\nu} = \frac{1}{2} \epsilon_{\mu\nu\lambda} \partial_{\nu} A_{\lambda}$  is the strength of the non-compact gauge field  $A_{\mu}$ .

It is easy to show that there are only 2 independent quartic invariants under the above transformations:

$$\Lambda_1 = |\psi_+|^4 + |\psi_-|^4, \quad \Lambda_2 = |\psi_+|^2 |\psi_-|^2$$
(9)

The direct honeycomb lattice is a non-Bravais lattice which contains two lattice points A and B per direct unit cell, it is useful to work out the rotation operators around the direct lattice points A and B which contain new symmetries not included in the rotation operator around a dual triangular lattice point  $R_{\pi/3}$ :

$$R_{2\pi/3}^{A} = \sum_{\vec{x}} e^{i2\pi f(a_2^2 - 2a_1 a_2 - 2a_1 - 2a_2)}$$

$$|-a_2 + 1, a_1 - a_2 > < a_1, a_2|$$

$$R_{2\pi/3}^{B} = \sum_{\vec{x}} e^{i2\pi f((a_2 - 1)^2 - 2a_1 a_2 + 2a_1)}$$

$$|-a_2 + 1, a_1 - a_2 + 1 > < a_1, a_2| \quad (10)$$

They act on the two vortex fields  $\psi_{\pm}$  as:

$$R_{2\pi/3}^A: \psi_{\pm} \to e^{\mp i\pi/3} \psi_{\pm}; \quad R_{2\pi/3}^B: \psi_{\pm} \to e^{\pm i\pi/3} \psi_{\pm}$$
 (11)

It is ease to see the two operators  $\Lambda_1$ ,  $\Lambda_2$  in Eqn.9 are also invariant under Eqn.11. Finally we reach the most general quartic term invariant under all the above transformations in Eqns.7, 11:

$$\mathcal{L}_4 = \gamma_0 (|\psi_+|^2 + |\psi_-|^2)^2 - \gamma_1 (|\psi_+|^2 - |\psi_-|^2)^2 \tag{12}$$

In the square lattice, in landau gauge, a unitary transformation to the permutative representation is needed to reach Eqn.12. Here in the gauge chosen in Eqn.3,  $\psi_{\pm}$  are automatically in the permutative representation. An important and subtle point is how to construct boson density order parameters to characterize the symmetry breaking patterns in the direct lattice in terms of the dual

vortex fields in the dual lattice. In<sup>4</sup>, the density order parameter was constructed to be the most general gauge invariant and bilinear combinations of the vortex fields  $\psi_l$ . Then it was evaluated at the direct lattice points, links and dual lattice points to represent boson density, kinetic energy and amplitude of the ring exchanges respectively. The dual lattice of a square lattice is still a square lattice with the same lattice constant. The link points of a square lattice also form a square lattice with lattice constant  $\sqrt{2}$ . Putting the direct, dual and link lattices together forms a square lattice with lattice constant 1/2. Although like a square lattice, the honeycomb lattice is also a bi-partisan lattice consisting of two interpenetrating triangular sublattices A and B, its dual lattice is a triangular lattice which is a frustrated one ( Fig.1), its link points form a Kagome lattice. Putting the three lattices together forms a very complicated lattice. So the density wave order parameters in the honeycomb lattice may not be evaluated in the three lattices. Indeed, when trying to identify the density operators in the insulating state, we find the density operators proposed in<sup>4</sup> does not apply anymore in the honeycomb lattice. In the following, by studying how gauge invariant bilinear vortex fields transform under the complete PSG, we can identify both the boson density and boson kinetic energy operators in the direct lattice. We need evaluate these quantities only at dual lattice points to characterize the CDW and VBS orders in the direct lattice. Let's look at the *generalized* density order operators which characterize the symmetry breaking patterns in the insulating states. In the low energy limit, the vortex field is  $\psi(\vec{x}) = e^{-i\vec{k}_+ \cdot \vec{x}} \psi_+(\vec{x}) + e^{-i\vec{k}_- \cdot \vec{x}} \psi_-(\vec{x})$ . Intuitively, the generalized density operator  $\rho(\vec{x}) = \psi^{\dagger}(\vec{x})\psi(\vec{x})$  can be

$$\rho(\vec{x}) = \psi_+^{\dagger} \psi_+ + \psi_-^{\dagger} \psi_- + e^{i\vec{Q}\cdot\vec{x}} \psi_+^{\dagger} \psi_- + e^{-i\vec{Q}\cdot\vec{x}} \psi_-^{\dagger} \psi_+ \tag{13}$$

where 
$$\vec{Q} = 2\pi/3(1,1)$$
.

When taking continuum limit on the dual lattice, we take one site per dual unit cell which contains two direct lattice sites A and B ( Fig. 1). So Eqn.13 should contain both the information on the boson densities on sites A and B and the boson kinetic energy on the link between A and B ( or XY exchange energy  $< S_A^+ S_B^- + h.c. >$  in the spin language ). The single boson Green function hopping on the direct lattice is related to the gauge-invariant single vortex Green function on the dual lattice in a highly non-local way<sup>23</sup>. Fortunately, the two boson quantities such as the density and the kinetic energy may have simple local expressions in terms of the dual vortex fields. By studying how the operators in Eqn. 13 transform under 7 and 11, in the scaling limit, we can identify these quantities as ( up to a unknown prefactor)<sup>24</sup>:

$$\rho_A = \psi_+^{\dagger} \psi_+, \quad \rho_B = \psi_-^{\dagger} \psi_- 
K_{AB} = e^{i\vec{Q} \cdot \vec{x}} \psi_+^{\dagger} \psi_- + e^{-i\vec{Q} \cdot \vec{x}} \psi_-^{\dagger} \psi_+$$
(14)

where  $\vec{x}$  stands for dual lattice points only.

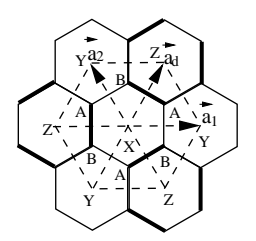


FIG. 1: (a) Bosons at filling factor f are hopping on a honeycomb lattice ( solid line ) which has two sublattices A and B. Vortices are hopping on its dual lattice which is a triangular lattice ( dashed line ) which has three sublattices X,Y,Z. In the easy-plane limit shown in Fig.2c, one of the three VBS states  $^{16}$  on the honeycomb lattice is shown by the thick bonds in the figure. The other two VBS can be obtained by  $R_{2\pi/3}^A$  or  $R_{2\pi/3}^B$ .

Moving slightly away from half filling f=1/2 corresponds to adding a small mean dual magnetic field  $H\sim \delta f=f-1/2$  in the action. It can be shown that inside the SF phase, the most general action invariant under all the MSG transformations upto quartic terms is .

$$\mathcal{L}_{SF} = \sum_{\alpha=a/b} |(\partial_{\mu} - iA_{\mu})\psi_{\alpha}|^{2} + r|\psi_{\alpha}|^{2} + \frac{1}{4e^{2}} (\epsilon_{\mu\nu\lambda}\partial_{\nu}A_{\lambda} - 2\pi\delta f\delta_{\mu\tau})^{2} + \mathcal{L}_{4}$$
 (15)

where  $A_{\mu}$  is a non-compact U(1) gauge field. Upto the quartic level, with correspondingly defined  $\psi_{a/b}$  in a square lattice, Eqn.15 is the same as that in the square lattice derived in<sup>4</sup>. Because Eqn.15 is a long wavelength effective action, the relations between the phenomenological parameters in Eqn.15 and the microscopic parameters in Eqn.1 are not known. Fortunately, we are still able to classify some phases and phase transitions and make some concrete predictions from Eqn.15 without knowing these relations. In the following, we assume r < 0 in Eqn.8, so the system is in insulating states. We will discuss the Ising limit and the easy-plane limit respectively.

## III. ISING LIMIT

If  $\gamma_1 > 0$ , the system is in the Ising limit, the mean field solution is  $\psi_a = 1, \psi_b = 0$  or vice versa. The system is in the CDW order. We can see how  $\rho_A, \rho_B$  transform under Eqns. 7 and 11:

$$T_{\alpha}, R_{2\pi/3}^{A/B}: \rho_{A/B} \to \rho_{A/B}; \quad R_{\pi/3}, I_{\alpha}: \rho_A \leftrightarrow \rho_B \quad (16)$$

These transformations confirm that  $\rho_A$  and  $\rho_B$  indeed can be identified as the boson density operators at direct sublattices A and B. In this section, we discuss at and away from half filling respectively.

(a) SF to CDW transition at half filling  $\delta f = 0$ . If r < 0, the system is in the CDW order which could

take checkboard  $(\pi,\pi)$  order 17. Eqn.15 is an expansion around the uniform saddle point  $<\nabla\times\vec{A}>=f=1/2$  which holds in the SF and the VBS ( to be discussed in section 4 ). In the CDW state, a different saddle point where  $<\nabla\times\vec{A}^a>=1-\alpha$  for sublattice A and  $<\nabla\times\vec{A}^b>=\alpha$  for sublattice B with  $\alpha<1/2$  should be used. Due to the change of the saddle point structures, the transition from the SF to the CDW driven by the horizontal axis ( quantum fluctuation r ) in Fig.2b is a strong first order transition.

(b) Charge Density Wave (CDW) supersolid away from half filling  $\delta f \neq 0$ . Now we look at the effects of the incommensurability  $\delta f = f - 1/2$  in Eqn.15. In the SF side where r > 0, it is known the SF is stable against the change of the chemical potential ( or adding bosons ). In the CDW side where r < 0, it is easy to see that there is only one vortex minimum  $\psi_b$  in the staggered dual magnetic field at  $\delta f = 0$ , the effective action inside the CDW state is:

$$\mathcal{L}_{CDW} = |(\partial_{\mu} - iA_{\mu}^{b})\psi_{b}|^{2} + \tilde{r}|\psi_{b}|^{2} + \tilde{u}|\psi_{b}|^{4} + \cdots + \frac{1}{4\tilde{\epsilon}^{2}}(\epsilon_{\mu\nu\lambda}\partial_{\nu}A_{\lambda}^{b} - 2\pi\delta f\delta_{\mu\tau})^{2}$$

$$(17)$$

where  $\tilde{r} < 0$ , so the system is in the CDW state, the vortices in the phase winding of  $\psi_b$  should be interpreted as the the boson number<sup>18</sup>. Note that the gauge field  $\tilde{A}^a$  is always massive, so it does not appear in Eqn.17.

Eqn.17 has the structure identical to the conventional q=1 component Ginzburg-Landau model for type-II " superconductors" in a "magnetic" field. It was shown in<sup>19</sup> that for type II superconductors, the gauge field fluctuations will render the vortex fluid phase intruding at  $H_{c1}$  between the Messiner and the mixed phase ( see Fig. 2a). For parameters appropriate to the cuprate superconductors, this intrusion occurs over too narrow an interval of H to be observed in experiments. In the present boson problem with the nearest neighbor interaction  $V_1 > 0$  in Eqn.1 which stabilizes the  $(\pi, \pi)$  CDW state at f = 1/2, along the dashed line driven by the vertical axis (chemical potential  $\mu$ ) in Fig.2b, this corresponds to a CDW supersolid (CDW-SS) state intruding between the commensurate CDW state at f = 1/2 and the in-commensurate CDW state at  $1/2 + \delta f$  which could be stabilized by further neighbor interactions in Eqn.1. The first transition is in the  $z=2, \nu=1/2, \eta=0$  universality class first discussed in<sup>1</sup>, while the second is a 1st order transition. We expect the intruding window at our q=2 system is much wider than that of the q=1 system. In the CDW states,  $\langle \psi_b \rangle \neq 0$ , so the dual gauge field  $\vec{A}_{\mu}^{b}$  in Eqn.17 is massive. In the CDW-SS state,  $<\psi_b>=0$ , there is the gapless superfluid mode represented by the dual gauge field  $A^b_\mu$ . The CDW-SS has the same  $(\pi, \pi)$  diagonal order as the C-CDW. The identified universality class of the CDW to the CDW-SS transition has many physical implications. For example, near the C-CDW to the CDW-SS transition, the superfluid density should scale as  $\rho_s \sim |\rho - 1/2|^{(d+z-2)\nu} = |\rho - 1/2| = \delta f$ 

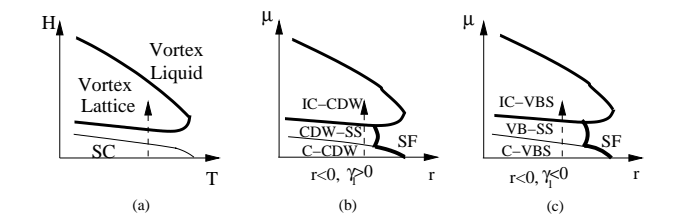


FIG. 2: (a) The phase diagram slightly away from q = 1 is the same as type-II superconductors in an external magnetic field H where there should be a vortex liquid state intruding between the Messiner state and the vortex lattice state. But the intruding regime is too narrow to be seen in type-II superconductors<sup>19</sup>. (b) and (c) are the zero temperature global phase diagrams of the chemical potential  $\mu$  versus r in Eqn.15 in the honeycomb lattice. (b) The Ising limit  $\gamma_1 > 0$ . There is a CDW supersolid (CDW-SS) state intruding between the commensurate CDW ( C-CDW ) state at f=1/2and the in-commensurate CDW (IC-CDW) state at  $1/2 + \delta f$ . The CDW-SS has the same lattice symmetry breaking as the C-CDW. (c) The Easy-Plane limit  $\gamma_1 < 0$ . There is a Valence Bond Supersolid (VB-SS) state intruding between the commensurate VBS (C-VBS) state at f = 1/2 and the incommensurate VBS ( IC-VBS ) state at  $1/2 + \delta f$ . The VB-SS has the same lattice symmetry breaking as the C-VBS. The thin (thick) line is the 2nd (1st) order transition. The 1st order transition in the Ising (Easy-plane) limit is strong ( weak ) one. (b) and (c) are drawn only above half filling.  $\mu \to -\mu$  corresponds to below half filling.

with a logarithmic correction. The logarithmic correction will be calculated in . There must be a transition from the CDW-SS to the SF inside the window driven by the quantum fluctuation r in the Fig.2b. The universality class of this transition is likely to be first order and will be investigated further in a future publication . Combining (3a) and (3b) leads to the global phase diagram Fig.2b in the Ising limit.

### IV. EASY-PLANE LIMIT.

If  $\gamma_1 < 0$ , the system is in the easy-plane limit, the mean field solution is  $\psi_a = e^{i\theta_a}, \psi_b = e^{i\theta_b}$ , then  $\rho_A = \rho_B = 1$ , so the two sublattices remain equivalent. This limit could be reached by possible ring exchange interactions in Eqn.1. In the following, we discuss at and away from half filling respectively.

(a) SF to VBS transition at half filling  $\delta f = 0$ . Because the two sublattices remain equivalent, the uniform saddle point  $\langle \nabla \times \vec{A} \rangle = f = 1/2$  holds in both the SF and the VBS. The system has a VBS order with the kinetic energy order parameter  $K_{AB} = \cos(\vec{Q} \cdot \vec{x} + \theta_{-})$  where  $\theta_{-} = \theta_{a} - \theta_{b}$ . Let's look at how the kinetic energy

K transform:

$$T_{\alpha} : K \to \cos(\vec{Q} \cdot (\vec{x} - \vec{a}_{\alpha}) + \theta)$$

$$R_{\pi/3} : K \to \cos(\vec{Q} \cdot \vec{x} - \theta); \quad I_{\alpha} : K \to K$$

$$R_{2\pi/3}^{A/B} : K \to \cos(\vec{Q} \cdot \vec{x} + \theta \mp 2\pi/3)$$
(18)

Note that K transforms differently under  $R_{\pi/3}$  and  $I_{\alpha}$ , because the latter are anti-unitary operators. These transformations confirm that K indeed can be identified as the boson kinetic energy or the XY exchange energy operators at the direct lattice.

Upto the quartic order, the relative phase between  $\psi_{+}$  and  $\psi_{-}$  is undetermined. Higher order terms are needed to determine the relative phase. It is clear to see there are only 3 sixth order invariants:

$$C_{1} = |\psi_{+}|^{6} + |\psi_{-}|^{6}$$

$$C_{2} = (|\psi_{+}|^{2} + |\psi_{-}|^{2})|\psi_{+}|^{2}|\psi_{-}|^{2}$$

$$C_{3} = (\psi_{+}^{*}\psi_{-})^{3} + (\psi_{-}^{*}\psi_{+})^{3} = \lambda \cos 3\theta$$
(19)

where  $\theta = \theta_+ - \theta_-$ . Especially  $C_3$  is invariant under  $R_{2\pi/3}^{A/B}$  Obviously, only the last term  $C_3$  can fix the relative phase. This term corresponds to the 3-monopole operator in the spin language.

If  $\lambda > 0, \theta = (2n+1)\pi/3 = \pi/3, \pi, -\pi/3$ . The kinetic energy K = 1, -2, 1 takes only two values, one strong bond and two weak bonds, their ratio is 2. The direct lattice can be divided into three sublattices X, Y, Z where  $x_1 + x_2 = 0, 1, 2 \mod 3$ , hence  $\vec{Q} \cdot \vec{x} = 0, 2\pi/3, -2\pi/3$  respectively (Fig.1). If we evaluate K at X, Y, Z, we find  $K_X = \cos \theta, K_Y = \cos(\theta + 2\pi/3), K_Z = \cos(\theta - 2\pi/3)$ . If we know one bond in one dual unit cell, say, labeled by X, then by the translation, we can get all the other bonds in sublattices Y and Z with the same orientation. The two bonds on the other two orientations can be reached by rotations listed in Eqn. 18. By this way, we can get all the bonds in the whole direct lattice. So the system is in the Valence Bond Solid (VBS) state, one VBS is shown in Fig.1.

If  $\lambda < 0, \theta = 2n\pi/3 = 0, 2\pi/3, -2\pi/3$ . The kinetic energy K = 2, -1, -1 takes also only two values, one strong bond and two weak bonds, their ratio is also 2. This case is essentially the same as  $\lambda > 0$ . Because the sign of the kinetic term can be changed in a bi-partisian lattice by changing the sign of  $b_i$  in one of the two sublattices in Eqn.1 (or can be changed by changing the sign of  $S_i^x, S_i^y$ in one of the two sublattices, but keeping  $S_i^z$  untouched in Eqn.2), but the product of the sign around a hexagon is fixed. The two cases have the same sign product, so can be transformed to each other by the transformation. This can also be understood by observing that  $C_3$  in Eqn.19 behaves like a hopping term in 3 power, so its sign can be changed by the transformation. This is in sharp contrast to the square lattice to be discussed in section V where one sign leads to a columnar dimer, the other leads to a plaquette pattern.

(b) Valence Bond Supersolid away from half filling  $\delta f \neq 0$ . Now we look at the effects of the in-

commensurability  $\delta f = f - 1/2$  in Eqn.15. Again, the SF side where r > 0 is stable against the change of the chemical potential. In the VBS side where r < 0, slightly away from the half-filling, Eqn.15 becomes:

$$\mathcal{L}_{VBS} = \left(\frac{1}{2}\partial_{\mu}\theta_{+} - A_{\mu}\right)^{2} + \frac{1}{4e^{2}}(\epsilon_{\mu\nu\lambda}\partial_{\nu}A_{\lambda} - 2\pi\delta f\delta_{\mu\tau})^{2} + \cdots + \left(\frac{1}{2}\partial_{\mu}\theta_{-}\right)^{2} + 2\lambda\cos3\theta_{-}$$

$$(20)$$

where  $\theta_{\pm} = \theta_a \pm \theta_b$ .

Obviously, the  $\theta_{-}$  sector is massive (namely,  $\theta_{a}$  and  $\theta_{b}$ are locked together ) and can be integrated out. Assuming  $\lambda > 0$ , then  $\theta_- = \pi$ . Setting  $\psi_+ = e^{i\theta_+} \sim \psi_a \sim -\psi_b$ in Eqn.15 leads to Eqn.17 with  $\tilde{u}=2\gamma_0$ , so the discussions on Ising limit case following Eqn.17 also apply. In the present boson problem with possible ring exchange interactions in Eqn.1 which stabilizes the VBS state at f = 1/2, along the dashed line driven by the vertical axis (chemical potential  $\mu$ ) in Fig.2c, this corresponds to a VBS supersolid (VB-SS) state intruding between the commensurate VBS (C-VBS) state at f = 1/2 and the in-commensurate VBS (IC-VBS) state at  $1/2 + \delta f$  as shown in Fig.2c. In this IC-VBS state,  $\delta f$  valence bonds shown in Fig.1 is slightly stronger than the others. In the VB-SS state,  $\langle \psi_a \rangle = \langle \psi_b \rangle = 0$ , but  $\langle \psi_a^{\dagger} \psi_a \rangle = \langle$  $\psi_b^{\dagger}\psi_b > = - \langle \psi_a^{\dagger}\psi_b \rangle \neq 0$ , so there is a VBS order characterized by the order parameter  $K_{AB} = \cos(\vec{Q} \cdot \vec{x} + \theta_{-})$ which is the same as the C-VBS. Again, the first transition is in the  $z=2, \nu=1/2, \eta=0$  universality class, while the second is 1st order. Near the C-VBS to the VB-SS transition, the superfluid density should scale as  $\rho_s \sim |\rho - 1/2|^{(d+z-2)\nu} = |\rho - 1/2| = \delta f$  with logarithmic corrections. The nature of the transition from the VB-SS to the SF where  $\langle \psi_a \rangle = \langle \psi_b \rangle = 0$  and  $\langle \psi_a^{\dagger} \psi_b \rangle = 0$ inside the window driven by the quantum fluctuation rin the Fig.2c is likely to be weakly first order and will be studied further in . Combining (4a) and (4b) leads to the global phase diagram Fig.2c.

#### V. SQUARE LATTICE.

As said below Eqn.15, with correspondingly defined  $\psi_{a/b}$  in a square lattice, upto the quartic level, Eqn.15 is the same as that in the square lattice derived in<sup>4</sup>. So the phase diagram in the Ising limit remains the same as Fig.2b. The SF to the C-CDW transition is a *strong* first order one. The IC-CDW can be stabilized only by very long range interactions in Eqn.1, if it is not stable, then Fig.2b reduces to Fig.14 in<sup>14</sup>. In the Easy-plane limit, as shown in<sup>4</sup>, the lowest order term coupling the two phases  $\theta_{a/b}$  is  $C_{sq} = \lambda \cos 4\theta$ , so the  $C_3$  term in Eqn.20 need to be replaced by  $C_{sq}$ . If  $\lambda$  is positive ( negative), the VBS is Columnar dimer ( plaquette ) pattern<sup>4</sup>.

By using duality analysis and QMC simulation, the author in 5 suggested that the q=2 component scalar electrodynamics Eqn.15 at  $\delta f=0$  in the easy plane limit is a

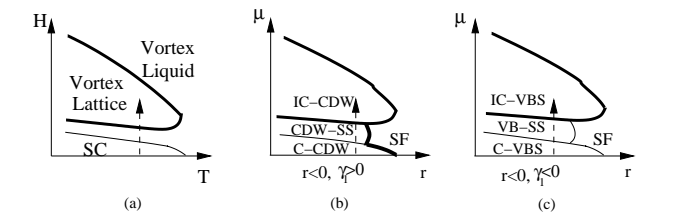


FIG. 3: Phase diagram in square lattice. (a) and (b) are similar to the honeycomb lattice in Fig.2. In the easy plane limit (c), there is a possible 2nd order transition between the SF and the C-VBS through a so called deconfined quantum critical point. However, this has been disputed in<sup>6</sup>.

second order transition through a so called "de-confined QCP". If this is indeed the case, then  $C_{sq} = \lambda \cos 4\theta$  is irrelevant, there is a possible 2nd order transition between the SF and the C-VBS through a so called deconfined quantum critical point. However, recently, by using QMC simulations at much larger systems, the authors in concluded that there is no such deconfined QCP, so the transition from SF to the VBS driven by the horizontal axis (quantum fluctuation r) in Fig.3c is a weak first order one. The phase diagram in the easy-plane limit remains the same as Fig.2c. The SF to the VBS transition remains a weak first order one.

## VI. IMPLICATION ON QUANTUM MONTE-CARLO (QMC) SIMULATIONS.

QMC simulations of hard core bosons on square lattice with  $V_1$  and  $V_2$  interactions find a stable striped  $(\pi,0)$ and  $(0,\pi)$  SS (Fig.4). A stable  $(\pi,\pi)$  SS can be realized in soft core boson case<sup>15</sup>. But the nature of the CDW to supersolid transition has never been addressed. Our results show that the CDW to the SS transition must be in the same universality class of Mott to superfluid transition with exact exponents  $z=2, \nu=1/2, \eta=0$ with a logarithmic correction. It is important to (1) confirm this prediction by finite size scaling through the QMC simulations in square lattice for  $(0, \pi)$  and  $(\pi, 0)$ supersolid in hard core case (Fig.14 in<sup>14</sup>) and  $(\pi, \pi)$  supersolid in the soft core case (2) do similar things in honeycomb lattice to confirm Fig.1. Some of the results are indeed confirmed in very recent QMC simulations on soft core bosons in honeycomb lattice $^{22}$ . (3) To Eqn.1 with  $U = \infty, V_1 > 0$ , adding a ring exchange term  $-K_s \sum_{ijkl} (b_i^{\dagger} b_j b_k^{\dagger} b_l + h.c.)$  where i, j, k, l label 4 corners of a square in the square lattice and  $-K_h\sum_{ijklmn}(b_i^{\dagger}b_jb_k^{\dagger}b_lb_m^{\dagger}b_n+h.c.)$  where i,j,k,l,m,n label 6 corners of a hexagon in the honeycomb lattice to stabilize the C-VBS state at half filling (  $K_s, K_h > 0$  are free of sign problem in QMC), then confirm the prediction on C-VBS to VB-SS transition in Fig.2c. The second transition (CDW-SS to IC-CDW in Fig.2b and the VB-

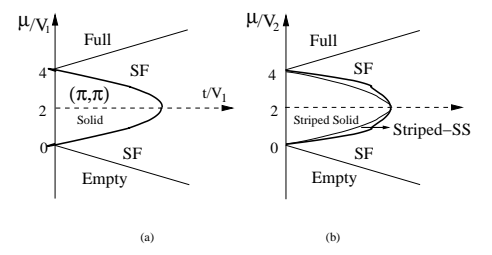


FIG. 4: The thin (thick) line is a 2nd (1st) order transition. (a), (b) are from QMC in<sup>14</sup>, but universality class of all the 2nd phase transitions in (b) was not studied in<sup>14</sup>.

SS to IC-VBS in Fig 2c is hard to be tested in QMC, because some very long range interactions are needed to stabilize the IC-CDW or the IC-VBS state. They are first order transition anyway.

In fact, one of the predictions in this paper on the scaling of the superfluid density  $\rho_s \sim |\rho-1/2|$  was already found in the striped  $(\pi,0)$  solid to striped supersolid transition by QMC in Sec.V-B<sup>14</sup>. As shown in section 4, there should be a logarithmic correction to the scaling of  $\rho_s$ , it remains a challenge to detect the logarithmic correction by a high precision QMC. Of course, the superfluid density is anisotropic  $\rho_s^x > \rho_s^y$  in the  $(\pi,0)$  supersolid, but they scale in the same way with different coefficients<sup>14</sup>. Although the authors in<sup>14</sup> suggested it is a 2nd order transition, they did not address the universality class of the transition.

In the following three sections, I will discuss the applications of the results achieved in the previous sections on 3 different experimental systems.

## VII. ULTRA-COLD ATOM ON SQUARE AND HONEYCOMB OPTICAL LATTICES

Recently, Bose-Einstein condensation (BEC) was realized in ultra-cold atomic gases (for a review, see<sup>28</sup>). Superfluid to Mott insulator transition was also observed in optical lattices of ultra-cold alkali atoms<sup>27</sup>. Atomic physicists are constructing effective various kinds of 2d and 3d optical lattices using laser beams and then load either ultra-cold fermion or boson atoms at different filling factors on the lattices. They may tune the parameters in Eqn.1 to realize different phases and quantum phase transitions<sup>27,28</sup>. The optical honeycomb lattice geometry Fig.1 and square lattice could be realized in future ultra-cold atomic experiments. The challenge is to achieve longer range interactions than the onsite interaction. Very exciting perspectives to achieve longer range interactions have been opened by recent experiments<sup>29</sup> on cooling and trapping of polar molecules. Being electrically or magnetically polarized, polar molecules interact with each other via long-rang anisotropic dipole-dipole interactions. Loading the polar molecules on a 2d optical lattice<sup>30</sup> with the dipole moments perpendicular to the trapping plane can be mapped to Eqn.1 with long-range repulsive interactions  $\sim p^2/r^3$  where p is the dipole moment. There are also other ways to generate long-range interactions<sup>31</sup>. We expect Fig.2a can be easily realized. There could also be some efficient ways to generate the ring exchange interactions<sup>31</sup> needed to stabilize the the VBS state in Fig.2b.

## VIII. ADATOM ADSORPTIONS ON SUBSTRATES ( HONEYCOMB LATTICE )

In this section, we will use the phase diagram Fig.2a to discuss two experimental systems: (1) the reentrant "superfluid" detected in a narrow region of coverages in the second layer of He4 ( called  ${}^4He/{}^4He/{}$ graphite system ) adsorbed on graphite by a previous torsional oscillator experiment ( ${}^{38}$ . (2) the reentrant "fluidlike" state of hydrogen adsorbed on Krypton-preplated graphite ( $H_2/Kr/graphite$ ) near half filling which was investigated in a recent experiment  ${}^{40}$ .

The dual vortex approach is a Magnetic Space Group (MSG) symmetry based approach which can be used to classify all the possible phases and phase transitions. However, the question if a particular phase will appear or not as a ground state depends on the specific values of all the possible parameters in the boson Hubbard model in Eqn.1, namely, the specific values in the real systems, it can not be addressed in this approach. There are two ways to remedy this short-coming. (1) we can compare our theoretical classifications with some known phases observed in experiments, then we can be more specific on our predictions on the nature of unknown phases and phase transitions. (2) As said in section VI, a microscopic approach such as Quantum Monte-Carlo (QMC) may be needed to supplement the dual field theoretical approach . In this section, we will take the first strategy to study the boson Hubbard model Eqn.1 in honeycomb lattice Fig.1 near q = 2 (Fig.1). The honeycomb lattice in Fig.1 may describe the preferred adsorption sites in the two systems. So the  ${}^4He/{}^4He/{}^4$ graphite and  $D_2/Kr/{}^2$ graphite systems may have the same symmetry and belong to the same universality class.

## A. ${}^{4}He/{}^{4}He/\text{graphite system}$

A superfluid is a fluid that flows through the tiniest channels or cracks without viscosity. So far, the phenomenon of superfluidity has been firmly observed in only two kinds of systems. The first system is the two isotopes of Helium:  ${}^4He$  and  ${}^3He$ . He4 is a boson and becomes a superfluid when  $T < T_c = 2.18K$ , while He3 is a fermion, two He3 atoms start to pair up when  $T < T_c = 2.4mK$  and form a superfluid  ${}^{32,33}$ . The second system is Bose-Einstein condensation in ultra-cold alkali atomic gases ( for a review, see  ${}^{28}$  ). Recently, intensive research activities have been lavished on searching for

excitonic superfluid in excitons in electron-hole semiconductor bilayers<sup>34</sup>. Torsional oscillator method was used to study <sup>4</sup>He films adsorbed on graphite<sup>38</sup>, a large Non-Classical Rotational Inertial (NCRI) was detected in a narrow window of coverages  $c=17\sim 19~atoms/nm^2$ in the second layer (  $^4He/{\rm \check{4}}He/{\rm graphite}$  system ). The NCRI is a low temperature reduction in the rotational moment of inertia due to the superfluid component of the state. This important phenomenon was interpreted as reentrant "superfluid" in this narrow window<sup>39</sup>. Recently, also by using the torsional oscillator measurement, a PSU group lead by Chan observed a marked  $1 \sim 2\%$ NCRI even in bulk solid  ${}^4He$  at  $\sim 0.2K^{10}$ . This was interpreted as a new state of matter called supersolid which has both superfluid order and crystalline order<sup>10</sup>. However, so far, no NCRI in bulk solid  $H_2$  was detected.

At the completion of the first layer, the  ${}^4He$  atoms with the coverage  $c \sim 12 \ atoms/nm^2$  form a triangular lattice which is incommensurate with the underlying graphite. It is reasonable to assume the lattice structure of the preferred adsorption sites on the second layer form a honeycomb lattice (Fig.1). When applying the Eqn.1 to the  ${}^4He/{}^4He/{}$ graphite system in Fig.1,  $b_i^{\dagger}$  is the  ${}^4He$ atom creation operator. The hopping amplitude t is determined by the trapping potential from the incommensurate first  ${}^4He$  layer. We assume the  ${}^4He$  atoms interact with each other with the LJ potential. Note that the LJ potential is quite accurate in describing the long distance attractive part, but very crude in the short distance repulsive part. The repulsive part in real case is expected to be softer. The chemical potential  $\mu$  determines the coverage. The filling factor f is related to the coverage c of  ${}^4He$  with  $c \sim 19.55 \ atoms/nm^2$  corresponding to f = 1/2 where one  ${}^4He$  atoms occupies every two lattice sites of the honeycomb lattice (for example, all the Asublattice sites ) to form a close packed triangular lattice with  $d_{AA} \sim 4.56 \text{Å}$  and  $d_{AB} \sim 2.63 \text{Å}$  which is just smaller than Lennard-Jones (LJ) parameter  $\sigma(^4He) \sim 2.64\text{Å}$ . The onsite U is very big. Because  $d_{AB} < \sigma_{^4He} < d_{AA}$ ,  $V_1$  is positive, while  $V_2$  and further neighbor interactions are weakly attractive and can be neglected. Note that our theoretical value  $19.55 \ atoms/nm^2$  is only 3% away from the experimental value 19  $atoms/nm^2$ . Fig.2a is very similar to the  $\rho_s$  versus  $c \sim f$  phase diagram in  ${}^{4}He/{}^{4}He/\text{graphite structure near }c=19 \text{ atoms/nm}^{2}$  ( see Fig. 1 in 38 ). The dashed line is the experimental path in  ${}^4He/{}^4He/{}$ graphite at T=0. Ir shows that a reentrant supersolid (SS) state is a generic state sandwiched between the C-IC transition. The reentrant " superfluid" state in the second layer of the  ${}^4He$  films adsorbed on graphite could be a <sup>4</sup>He supersolid state. Very interestingly, the data in the torsional oscillator experiment in<sup>38</sup> do not show the characteristic form for a 2d <sup>4</sup>He superfluid film, instead it resemble that in <sup>10</sup> characteristic of a possible supersolid in terms of the gradual onset temperature of the NCRI, the unusual temperature dependence of  $T_{SS}$  on the coverage. From Fig.2a, it is easy to see that it maybe difficult to reach the superfluid by moving along the horizontal r axis, but it is very easy to get to the CDW-SS state by moving along the vertical coverage axis. In principle, there should be a Kosterlitz-Thouless (KT) finite temperature phase transition above which the CDW-SS becomes a coexistence of the CDW state and normal fluids of interstitials. The effects of disorders on this finite temperature transition will be studied in and compared with Fig.2 and 3 in<sup>38</sup>.

## B. $H_2/Kr/graphite$ system

There are great interests in finding superfluidity in other substances. Hydrogen molecules are relatively light, quantum fluctuations are large at very low temperature. a para-H2 molecule is a boson and very similar to a He4 atom, in principle, H2 could become superfluid at low temperature as He4 does. Unfortunately, unlike He4, due to deeper attractive potentials, bulk H2 solidifies at low temperature ( $T_c \sim 14K$ ), this preempts the possible observation of the speculated superfluity. At sufficiently high pressure, the solid hydrogen will transform into a metallic alkali-like crystal or an unusual two component (protons and electrons) quantum liquid at low temperatures<sup>37</sup>. Potential avenues to prevent p-H2 from being solidified to low enough temperature such that the superfluid behaviour can be observed is by decreasing the average number of neighbors of a H2 molecule. Monte Carlo simulations of  $H2_n$  clusters with n = 13 - 18showed that there is indeed a tendency for the system to be superfluid below 1K<sup>35</sup> Indeed, Infra-red spectroscopy also provided evidences for superfludity in  $o(D_2)_n$  and  $p(H_2)_n$  clusters with  $n = 14 - 17^{36}$ . Another route is by the reduction of dimensionality. Extensive theoretical and experimental work has been devoted to study H2 and D2 films in a variety of substrates. Path Integral Monte-Carlo (PIMC) simulations indicated that introduction of certain impurities can stabilize a 2 dimensional liquid hydrogen which undergoes a Kosterlitze-Thouless (KT) transition below 1.2 K.

In a recent experiment, neutron scattering measurements were used to characterize all the possible phases of  $D_2$  coadsorbed on graphite preplated by a monolayer of Kr called  $D_2/\text{Kr/graphite structure}^{40}$ . Because two dimensional graphite has the honeycomb net structure, the corresponding preferred adsorption sites form a triangular lattice. The precoated Kr atoms will occupy the preferred adsorption sites and form a triangular lattice. Then the  $D_2$  deposited on top of the Kr monolayer will sit on the preferred adsorption sites of the triangular lattice of the Kr monolayer to form a honeycomb lattice. So, the lattice geometry is very similar to Fig.1 with Kr atoms sitting on the triangular lattice, while the  $H_2$  molecules hopping on the honeycomb lattice. The filling factor f is related to the coverage c of  $D_2$ . In the coverage c verse the temperature T phase diagram, an unusual feature is that in a small coverage range ( 1.20 < c < 1.25 ) at the commensurate-incommensurate (C-IC) transition,

a reentrant fluid phase squeezes in between the C and IC phases down to T = 1.5 K which is the lowest temperature a liquidlike phase of  $D_2$  has ever been found. The filling factor f is related to the coverage c of  $H_2$ with c = 1.2 corresponding to f = 1/2 where one  $H_2$ molecule occupies every two lattice sites of the honeycomb lattice with  $d_{AA} \sim 3.87 \text{Å}$  and  $d_{AB} \sim 2.24 \text{Å}$  in Fig.1. Because  $d_{AB} < \sigma_{H_2} < d_{AA}$ ,  $V_1$  could also be positive and very big, while  $V_2$  and further neighbor interactions are weakly attractive, the above discussions on <sup>4</sup>He in subsection A can also be applied to this system. Fig.2a is very similar to the  $c \sim f$  versus low T phase diagram in  $H_2/Kr/graphite$  structure near c = 1.20 ( Fig. 6 in<sup>40</sup>). The dashed line is the experimental path in  $H_2/\mathrm{Kr/graphite}$  at T=0. The so called  $(1\times 1)[\frac{1}{2}]$ commensurate phase in<sup>40</sup> is the CDW state where the  $D_2$  atoms occupy one of the two sublattices of the underlying honeycomb lattice. The transition at zero temperature is a C-CDW to CDW-SS to IC-CDW transition described by Fig.2(a). The first transition is in the  $z=2, \nu=1/2, \eta=0$  universality class. Because  $\nu<1$ , from Harris criterion, disorders are relevant. The second transition is first order. It suggests the reentrant " fluidlike" phase could be the  $H_2$  supersolid. If this is indeed the case, this may lead to the first observation of  $H_2$  supersolid. Torsional oscillator experiment similar to that used in<sup>38</sup> may be used to measure the NCRI of this  $H_2$  supersolid state. Obviously, this experiment can avoid the difficulty of using  $D_2$  which has large coherent neutron scattering cross section, but smaller de Boer quantum number. In fact, Kr may not be the best spacer to observe the  $H_2$  supersolid state. The ideal situation is to make  $d_{AB}$  is just slightly smaller than  $\sigma_{H_2}$ . Larger atoms like  $Xe, CF_4, SF_6$  may be more suitable spacers, because they may increase the distance  $d_{AB}$  in the Fig.1 just slightly smaller than  $\sigma_{H_2}$ . We suggest that  ${}^{4}He$  supersolid should also appear in, for example, <sup>4</sup>He/Kr/graphite structure.

The reentrant lattice SS discussed in this section is different from the bulk  ${}^4He$  SS state discussed in  ${}^{11}$ , although both kinds of supersolids share many interesting common properties. In the former, there is a periodic substrate or spacer potential which breaks translational symmetries at the very beginning. While in the latter, the lattice results from a spontaneous translational symmetry breaking, so the theory developed in this paper on lattices is completely different from the continuum theory developed in  ${}^{11}$ . Combined with the results in  ${}^{11}$ , we conclude that  ${}^4He$  supersolid can exist both in bulk and on substrate, while although  $H_2$  supersolid may not exist in the bulk, but it may exist on wisely chosen substrates. Ultra-cold atoms supersolid could also be realized in optical lattices.

# IX. COOPER-PAIR SOLID, SUPERFLUID AND COOPER-PAIR SUPERSOLID IN HIGH TEMPERATURE SUPERCONDUCTORS ( SQUARE LATTICE)

Very recently<sup>41</sup>, by using both angle resolved photoemission (ARPES) and scanning tunneling microscopy (STM) on high temperature superconductor  $La_{2-x}Ba_xCuO_4^{42,43}$ , Valla et.al detected a quasi-particle energy gap with d-wave symmetry even when the superconductivity is completely suppressed at x = 1/8, while having almost equally strong superconducting phases at both higher and lower dopings (Fig.5). The gap turns out to reach maximum at x = 1/8 despite  $T_c \to 0$  at x = 1/8. This fact suggests that the most strongly bound Cooper pairs at x = 1/8 are most susceptible to the charge density wave (CDW) ordering which suppresses  $T_c \to 0$ . In this section, I propose that the formation of a stripe Cooper pair supersolid may be able to explain the very unusual phase diagram of  $La_{2-x}Ba_xCuO_4$  at and near doping level x = 1/8.

The fact that the STM and ARPES measurements in<sup>41</sup> still detected an energy gap at Fermi surface with  $d_{x^2-y^2}$  wave symmetry suggests that there are tightly bound Cooper pairs in this cuprate. We can treat these Cooper pairs as bosons, therefore many important results achieved in previous sections on interacting bosons hopping on lattices maybe applied to this cuprate. One important new feature for tightly bound Cooper pairs is that they carry charges 2e, therefore interact with bare long-range Coulomb interaction (in high  $T_c$  cuprates, by taking the penetration depth  $\lambda \to \infty$ , one can neglect the very weak Meissner effect )<sup>3</sup>. I propose the following physical picture: at exactly x = 1/8, the filling factors of the bosons on the square lattice is  $f = \frac{1-x}{2} = 7/16$ , the system is a CDW (more specifically, stripe) of Copper pairs with 4 sites per unit cell, so  $T_c = 0$ . Then we need q = 16 dual vortices to describe the stripe CDW in the dual vortex picture. It was explicitly pointed out in section III that special care is needed to choose the correct saddle point of the dual gauge field  $A_{\mu}$  to describe this stripe CDW state. Slightly away from x = 1/8, on both sides, the groundstate is a Stripe Cooper pair supersolid (CP-SS)! When x > 1/8 (x < 1/8), it is a hole ( electron ) doped stripe CP-SS. Indeed, as shown by Quantum Monte-Carlo simulation<sup>14</sup>, only striped supersolid is stable in a square lattice for hardcore bosons. The quantum phase transition from the stripe Cooper pair solid to the stripe CP-SS driven by the doping is in the same universality class as that from a Mott insulator to a superfluid, therefore have exact exponents  $z=2, \nu=1/2, \eta=0$  (with possible logarithmic corrections ). The resulting stripe CP-SS has the same lattice symmetry breaking patterns as the stripe Cooper pair solid with the superfluid density scaling as  $\rho_s \sim |x - 1/8|^{(d+z-2)\nu} = |x - 1/8| = |\delta x|$  with a possible logarithmic correction. As pointed out in section III, the superfluid density is anisotropic with  $\rho_s$  along the stripe

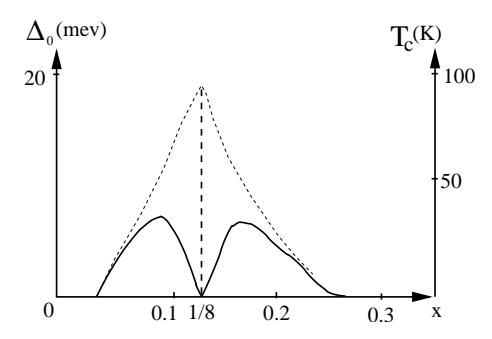


FIG. 5: The dashed line is the energy gap  $\Delta_0$  which reaches minimum at x = 1/8, the solid line is the superconducting transition temperature  $T_c$  which has two domes and is zero at x = 1/8.

is larger than that normal to the stripe, but both scale in the same way with different coefficients. From Uemura relation, we conclude that  $T_c \sim |\delta x|$  ( in fact, it scales as the smaller  $\rho_s$  in the Stripe CP-SS ). This result very naturally explains why  $T_c$  indeed looks linear in  $|\delta x|$  and the phase diagram is nearly symmetric near x=1/8 found in  $^{41}$ .

The above picture only involves the sector of the tightly bound Copper pair. Of course, understanding the ground state of the Cooper-pair sector is very important on its own and is also the starting point to incorporate quasi-particles<sup>45,46,47</sup> and spin excitations<sup>48</sup> into the picture. As shown in section IV, a valence-bond supersolid (VB-SS) can be stabilized if there is a considerable ring exchange interaction. An interesting question to address is if valence-bond Cooper-pair supersolid can be realized in some of these cuprates.

#### X. CONCLUSIONS

By using the DVM, we studied superfluid, solid and supersolid and quantum phase transitions of the extended boson Hubbard model near half filling on bipartite optical lattices such as honeycomb and square lattice and mapped out the global phase diagram at T=0 in a unified scheme. We identified boson density and boson kinetic energy operators in terms of the dual vortex fields to characterize symmetry breaking patterns in the insulating states and supersolid states. We found that in the insulating side, the transition at zero temperature driven by the chemical potential must be a C-CDW ( or C-VBS ) at half filling to a narrow window of CDW- ( VB-) supersolid, then to a IC-CDW (IC-VBS) transition in the Ising (easy-plane) limit. The valence bond supersolid is a new kind of supersolid first proposed in this paper. The first transition is in the same universality class as that from a Mott insulator to a superfluid driven by a chemical potential, therefore have exact exponents  $z=2, \nu=1/2, \eta=0$  with a logarithmic correction. The second is a 1st order transition. The results

achieved in this letter could guide QMC simulations to search for all these phases and confirm the universality class of the transitions. The EBHM in honeycomb and square lattices could be realized in ultracold atoms loaded on optical lattices. So the results achieved in this paper may have direct impacts on the atomic experiments in optical lattices. Then we applied the results to two condensed matter experimental systems: (1) adatom adsorption on different substrates such as the adsorption in the second layer of  ${}^4He$  adsorbed on graphite and Hydrogen adsorbed on Krypton-preplated graphite in honeycomb lattice, we find that a reentrant  ${}^{4}He$  supersolid in the second layer on graphite may be responsible for the NCRI detected in the torsional oscillator experiments  $in^{38}$  and a reentrant  $H_2$  supersolid at T=0 maybe responsible for the reentrant liquid state squeezed between C and IC phases detected by coherent neutron scattering. We propose that a judicious choice of substrate may also lead to an occurrence of hydrogen lattice supersolid. (2) superconducting phase diagram near x = 1/8 in high temperature superconductor  $La_{2-x}Ba_xCuO_4$  in square lattice. We conclude that there is a stripe CDW at 1/8 which suppresses  $T_c$  to zero. There are hole and electron doped Cooper pair supersolids on both sides of x=1/8 which has the same lattice symmetry breaking pattern as the stripe CDW at x=1/8 and with  $\rho_s \sim T_c \sim |x-1/8|$ . Although the SS in lattice models is different from that in a continuous systems, the results achieved in this paper on lattice supersolids may still shed some lights on the possible microscopic mechanism and phenomenological Ginsburg-Landau theory of the possible  $^4He$  supersolids  $^{11}$ .

I thank Milton Cole for pointing out the experiment in Ref. 40 to me. This research at KITP was supported in part by the NSF under Grant No. PHY99-07949 at KITP-C by the Project of Knowledge Innovation Program (PKIP) of Chinese Academy of Sciences. I also thank Chang-pu Sun for hospitality during my visit at KITP-C.

- <sup>1</sup> M. P. A. Fisher, P. B. Weichman, G. Grinstein and D. S. Fisher; Phys. Rev. B 40, 546 (1989).
- <sup>2</sup> M. P. A. Fisher and G. Grinstein, Phys. Rev. Lett. 60, 208 (1988).
- <sup>3</sup> Jinwu Ye, Phys. Rev. B 58, 9450-9459 (1998).
- <sup>4</sup> L. Balents, et.al Phy. Rev. B 71, 144508 (2005).
- O.I. Motrunich and A. Vishwanath, Phys. Rev. B 70, 075104 (2004); T. Senthil, Ashvin Vishwanath, Leon Balents, Subir Sachdev, M. P. A. Fisher, Science 303, 1490 (2004); cond-mat/0312617.
- <sup>6</sup> A. Kuklov, N. Prokof'ev, B. Svistunov, Matthias Troyer, cond-mat/0602466.
- C. Dasgupta and B. I. Halperin , Phys. Rev. Lett. 47, 1556-1560 (1981), David R. Nelson, Phys. Rev. Lett. 60, 1973-1976 (1988); Matthew P. A. Fisher and D. H. Lee, Phys. Rev. B 39, 2756-2759 (1989).
- Bouglas R. Hofstadter, Phys. Rev. B 14, 2239-2249 (1976).
   J. Zak, Phys. Rev. 134, A1602-A1606 (1964), Phys. Rev. 134, A1607-A1611 (1964).
- <sup>10</sup> E. Kim and M. Chan, Science 24, 1941 (2004).
- <sup>11</sup> Jinwu Ye, Phys. Rev. Lett. 97, 125302 (2006), cond-mat/0705.0770, cond-mat/0603269.
- <sup>12</sup> G. Murthy, D. Arovas, A. Auerbach, Phys. Rev. B 55, 3104 (1997).
- <sup>13</sup> G. C. Batrounil *et al*, Phys. Rev. Lett. 74, 2527 (1995); *ibid*, 84, 1599 (2000).
- <sup>14</sup> F. Hebert, et al; Phys. Rev. B, 65, 014513 (2001).
- <sup>15</sup> P. Sengupta, et al, Phys. Rev. Lett. 94, 207202 (2005).
- P.W. Anderson; Science 235, 1196(1987); N. Read and S. Sachdev, Phys. Rev. Lett. 62, 1694 (1989); Phys. Rev. B42, 4568 (1990).
- <sup>17</sup> The discussions in the following equally apply to the striped solid with  $(\pi,0)$  or  $(0,\pi)$  order with the exception of the anisotropy in the superfluid density. The anisotropy is irrelevant to the universality class.
- In the direct lattice picture, we can simply renormalize away the sublattice A where the bosons sit and focus on

- the effective boson hopping on the sublattice B whose dual vortex action is given by Eqn.17.
- <sup>19</sup> D. S. Fisher, M. P. A. Fisher and D. A. Huse, Phys. Rev. B 43, 130 (1991).
- <sup>20</sup> Jinwu Ye, cond-mat/0503113.
- <sup>21</sup> Longhua Jiang and Jinwu Ye, J. Phys, Condensed Matter. 18 (2006) 6907-6922.
- <sup>22</sup> Jing Yu Gan, Yu Chuan Wen, Jinwu Ye, Tao Li, Shi-Jie Yang, Yue Yu, Phys. Rev. B 75, 214509 (2007).
- <sup>23</sup> Jinwu Ye, Phys. Rev. B 67, 115104 (2003); J. Phys. Condens. Matter 16 (2004) 4465-4476.
- <sup>24</sup> In quantum impurity problems, in the scaling limit, the impurity degree of freedoms disappear and are replaced by operators with the same symmetry, see, for example, Jinwu Ye; Phys. Rev. Lett. 79, 1385 (1997).
- $^{25}$  In principle, the  $\delta f$  should be the chemical potential.
- Similar quantum phase transitions induced by bias volatge may appear in im-balanced Bi-layer Quantum Hall systems, Jinwu Ye, Phys. Rev. Lett. 97, 236803 (2006).
- <sup>27</sup> M. Greiner, et al, Nature 415, 39-44 (2002).
- <sup>28</sup> F. Dalfovo, S. Giorgini, L. P. Pitaevskii and S. Stringari, Rev. Mod. Phys. 71, 463C512 (1999).
- <sup>29</sup> Jeremy M. Sage,1 Sunil Sainis,1 Thomas Bergeman,2 and David DeMille1, Phys. Rev. Lett. 94, 203001 (2005), T. Rieger, T. Junglen, S. A. Rangwala, P. W. H. Pinkse, and G. Rempe, Phys. Rev. Lett. 95, 173002 (2005). M. A. Baranov,1,2,3 Klaus Osterloh,1 and M. Lewenstein1, Phys. Rev. Lett. 94, 070404 (2005). J. Stuhler,1 A. Griesmaier,1 T. Koch,1 M. Fattori,1 T. Pfau,1 S. Giovanazzi,2 P. Pedri,3 and L. Santos3, Phys. Rev. Lett. 95, 150406 (2005).
- <sup>30</sup> K. Gral, L. Santos, and M. Lewenstein, Phys. Rev. Lett. 88, 170406 (2002).
- <sup>31</sup> H. P. Bchler, M. Hermele, S. D. Huber, Matthew P. A. Fisher, and P. Zoller, Phys. Rev. Lett. 95, 040402 (2005).
- <sup>32</sup> P. Kapitza, Nature 141, 74 (1938).
- <sup>33</sup> D. D. Osheroff, R. C. Richardson, and D. M. Lee, Phys. Rev. Lett. 28, 885C888 (1972)

- <sup>34</sup> Jinwu Ye, preprint.
- <sup>35</sup> P. Sindzingre, D. M. Ceperley and M. L. Klein, Phys. Rev. Lett. 67, 1871C1874 (1991).
- <sup>36</sup> Slava Grebenev, Boris Sartakov, J. Peter Toennies, and Andrei F. Vilesov, Science 1 September 2000; 289: 1532-1535
- <sup>37</sup> Stanimir A. Bonev, Eric Schwegler, Tadashi Ogitsu, Giulia Galli, Nature 431, 669 672 (07 Oct 2004).
- <sup>38</sup> P. A. Crowell and J. D. Reppy, Phys. Rev. Lett. 70, 3291C3294 (1993); Phys. Rev. B 53, 2701C2718 (1996).
- <sup>39</sup> The possibility of supersolid was briefly mentioned in the second reference in<sup>38</sup>. P. A. Crowell and J. D. Reppy, private communications.
- <sup>40</sup> Horst Wiechert and Klaus-Dieter Kortmann, Norbert Ster, Phys. Rev. B 70, 125410 (2004).
- <sup>41</sup> T. Valla, A. V. Fedorov, Jinho Lee, J. C. Davis, G. D. Gu,

- Vol. 314. no. 5807, pp. 1914 1916. Science 22 December 2006
- <sup>42</sup> J. G. Bednorz and K. A. Muller, Z. Phys. B 64, 189 (1986)
- <sup>43</sup> A. R. Moodenbaugh, Youwen Xu, and M. Suenaga, T. J. Folkerts and R. N. Shelton, Phys. Rev. B 38, 4596 4600 (1988).
- <sup>44</sup> J. M. Tranquada, H. Woo, T. G. Perring, H. Goka, G. D. Gu, G. Xu, M. Fujita, K. Yamada, Nature 429, 534 538 (03 Jun 2004).
- <sup>45</sup> Jinwu Ye and S. Sachdev, Phys.Rev.B, 10173 (1991).
- <sup>46</sup> Jinwu Ye, Phys. Rev. Lett. 86, 316 (2001).
- <sup>47</sup> Jinwu Ye, Phys. Rev. Lett. 87, 227003 (2001).
- <sup>48</sup> A. V. Chubukov, S. Sachdev and Jinwu Ye, Phys. Rev. B 49, 11919 (1994).